PALEONTOLOGY

The Rise of Algae promoted eukaryote predation in the Neoproterozoic benthos

Daniel B. Mills[1,2]*, Aurèle Vuillemin[3], Katharina Muschler[1], Ömer K. Coskun[1], William D. Orsi[1,4]*

The proliferation of marine algae in the Neoproterozoic Era is thought to have stimulated the ecology of predatory microbial eukaryotes. To test this proposal, we introduced algal particulate matter (APM) to marine sediments underlying a modern marine oxygen minimum zone with bottom-water oxygen concentrations approximating those of the late Neoproterozoic water column. We found that under anoxia, APM significantly stimulated microbial eukaryote gene expression, particularly genes involved in anaerobic energy metabolism and phagocytosis, and increased the relative abundance of 18*S* rRNA from known predatory clades. We additionally confirmed that APM promoted the reproduction of benthic foraminifera under anoxia with higher-than-expected net growth efficiencies. Overall, our findings suggest that algal biomass exported to the Neoproterozoic benthos stimulated the ecology of benthic predatory protists under anoxia, thereby creating more modern food webs by enhancing the transfer of fixed carbon and energy to eukaryotes occupying higher trophic levels, including the earliest benthic metazoans.

INTRODUCTION

Crown-group eukaryotes—the clade encompassing the last eukaryote common ancestor (LECA) and all of its descendants—apparently diversified in the Neoproterozoic Era (1000 to 539 million years ago or Ma) (*1*, *2*), before the establishment of modern marine oxygen (O_2) levels (*3*). While the oldest body fossils with diagnostic eukaryote features date to ~1650 Ma (*1*), body fossils confidently assigned to living eukaryote lineages are unknown from rocks older than ~1050 Ma (*4*). Similarly, extractable regular (4-desmethyl) steranes—the molecular fossils of sterols produced by living eukaryotes—are unknown from rocks older than ~820 Ma (*2*, *5*, *6*), although the remains of sterol precursors are known from rocks as old as ~1640 Ma (*2*). The succession of the earliest extractable steranes in the rock record suggests an increase in the relative abundance of marine red algae (members of the Rhodophyta in the Archaeplastida supergroup) by ~820 Ma, followed by an increase in the relative abundance of marine green algae (members of the Chloroplastida in the Archaeplastida supergroup) by ~635 Ma (*2*, *6*). These shifts correspond to increased ratios of steranes to hopanes (the molecular fossils of bacterial hopanoids), suggesting a growing contribution of algal versus bacterial organic matter to marine sediments throughout this interval (*5*). Together, this apparent expansion of marine archaeplastids in the Neoproterozoic ocean has been broadly referred to as the "Rise of Algae" (*5*).

The oldest body fossil evidence for modern eukaryote primary producers, as well as the biomarker evidence for the Rise of Algae, broadly corresponds to the oldest body fossil evidence for eukaryote-on-eukaryote predation (eukaryovory) (*7*). Some of the oldest body fossils displaying signs of eukaryote predation (*8*) have been confidently assigned to extant groups of heterotrophic microbial eukaryotes (protists), namely the Amoebozoa (*9*), while other fossils from the same locality (770 to 742 Ma) have been more tentatively assigned to the Rhizaria, specifically the Cercozoa (*8*). Younger body fossils from 716 to 635 Ma have also been interpreted as the potential remains of rhizarians, specifically the Foraminifera (*10*). It has also been proposed that C_{30} steranes from the Cryogenian Period (720 to 635 Ma) were sourced from rhizarians (*11*), consistent with body fossil evidence for foraminifera and cercozoans by this time, although these steranes are also interpreted as the remains of demosponges (*12*), algae (*13*), and bacteria (*14*). Overall, the body fossil and lipid biomarker records have inspired the prediction that the Rise of Algae promoted the growth of eukaryovorous protists, which, in turn, escalated predator-prey dynamics, such as actively selecting for larger body sizes among eukaryotic prey, including the unicellular-colonial ancestors of macroalgae and metazoans (*5*, *11*, *15*). In addition, the Rise of Algae likely enhanced the flux of carbon, energy, and nutrients from eukaryote primary producers to the Neoproterozoic benthos, stimulating the trophic ecology of the earliest benthic animals (metazoa), which unequivocally entered the fossil record by the Ediacaran Period (635 to 539 Ma) (*16*). Despite the apparent plausibility of these proposed scenarios, the effect of sinking algal matter on eukaryotic predation in the benthos remains largely unconstrained by observations of modern ecosystems. Furthermore, eukaryovorous protists like foraminifera and ciliates are often assumed by paleontologists and geochemists to have been "near-absent" in anoxic environments in the Neoproterozoic (*17*, *18*), despite widespread evidence for their activity in anoxic systems today (*19*–*24*), suggesting a potentially overlooked role of anaerobic benthic phagotrophs during the Rise of Algae. Determining how the Rise of Algae most likely affected the evolution of Neoproterozoic ecosystems requires explicitly testing predictions based on the rock record against data gathered from modern marine organisms and environments.

The microbial loop and anaerobic food webs

In modern ecosystems, fixed carbon is both remineralized and channeled to higher trophic levels—namely the metazoans of "classic food chains"—by microorganisms in what is called the "microbial loop," a hallmark of modern oceanography (*25*). Within the microbial loop, protists in particular channel the carbon and energy of primary producers (e.g., autotrophic bacteria and algae) to metazoans by preying

[1]Department of Earth and Environmental Sciences, Paleontology and Geobiology, Ludwig-Maximilians-Universität München, 80333 Munich, Germany. [2]The Penn State Extraterrestrial Intelligence Center, Penn State, University Park, PA 16802, USA. [3]GFZ German Research Centre for Geosciences, Section Geomicrobiology, Telegrafenberg, 14473 Potsdam, Germany. [4]GeoBio-Center[LMU], Ludwig-Maximilians-Universität München, 80333 Munich, Germany.
*Corresponding author. Email: d.mills@lmu.de (D.B.M.); w.orsi@lrz.uni-muenchen.de (W.D.O.)

upon bacteria, archaea, and other microbial eukaryotes via phagocytosis (or "cell eating"). In the global ocean today, protists are thought to consume up to 62% of algal primary production daily (*26*) and are even known to acquire mixotrophy (the capacity for both heterotrophy and phototrophy) by retaining the plastids of algal prey (*27*). While the Rise of Algae would have likely promoted protist-on-algal predation in oxic marine surface waters in the Neoproterozoic, the processing of exported algal matter by anaerobic protists living in anoxic marine sediments has received little-to-no attention, hindering our understanding of how the Rise of Algae would have transformed the base of the marine food web within the Neoproterozoic benthos.

In the modern ocean, free-living anaerobic protists are common in both benthic and planktonic habitats where O_2 is undetectable (*19*, *20*). The gross growth efficiency [yield = (assimilated carbon)/(consumed carbon)] of anaerobic (fermentative) food chains is estimated to be 10%—four times less than the 40% gross growth efficiency of aerobic food chains (*28*). In other words, for every four units of carbon transferred from one trophic level to the next in aerobic food chains, only one unit of carbon is transferred in anaerobic food chains, potentially explaining the lower number of trophic levels and protist-to-bacteria biomass ratios of anoxic ecosystems (*28*). The comparatively low growth efficiencies of anaerobic protists, however, can be compensated for by increasing the cell size and therefore the carbon and energy content, of microbial prey, resulting in higher growth rates than those expected based on gross growth efficiency alone (*29*). As a result, it is possible that the growing input of algal versus cyanobacterial biomass to anoxic marine sediments during the Neoproterozoic enhanced the growth rates of anaerobic benthic protists, which, in turn, could have promoted the transfer of carbon and energy to additional trophic levels, such as those occupied by the earliest animals. To better understand the effects of exported algae on anaerobic protists in the benthos, we performed algal-predation experiments in marine sediments under both oxic and anoxic conditions.

The Benguela Upwelling System

Our study site was the Benguela Upwelling System (BUS) located along the western coast of southern Africa (see Materials and Methods). The BUS is the most productive of the four main Eastern Boundary Currents with an estimated primary production rate of 0.37 Gt C per year (*30*). The upwelling of nutrient-rich waters in response to offshore Ekman transport fuels this elevated productivity, which, coupled to the physical stratification of the water column in summer, produces a seasonally fluctuating oxygen minimum zone extending to the seafloor. Common primary producers in the BUS include both toxic and nontoxic bloom-forming dinoflagellates (e.g., *Noctiluca scintilans*), phototrophic ciliates (e.g., *Mesodinium rubrum*), and diatoms (e.g., members of the genus *Chaetoceros*) (*31*–*34*). The sediments underlying the BUS form a mixture of diatomaceous ooze and foraminifera sand (*35*) and exhibit abundant and active benthic foraminifera with anaerobic energy metabolisms (*22*). At the time of sampling, dissolved O_2 was detectable throughout the water column with concentrations ranging from 20 to 40 μM (8 to 16% of atmospheric saturation) in the bottom waters directly overlying the benthos (110- to 127-m depth) (*22*). The sediments immediately below (0 to 30 cm) the seafloor were characterized by anoxia (undetectable O_2) and H_2S concentrations ranging from 0 to 12 μM (*22*). To assess the response of benthic microbes to the influx of exported algae, we added seafloor sediment and algal particulate matter (APM) to gas-tight glass flasks and monitored the microbial response over time compared to control flasks without added APM (see Materials and Methods).

RESULTS

Anaerobic protist gene expression stimulated by algal input

In the water phase of our flasks, O_2 was initially present and was consumed in the presence of APM until it fell below detection (reaching anoxia) by ~22 hours, while O_2 remained detectable in the no-APM controls for no longer than 28 hours (fig. S1). During the final two time points (7 and 10 days), O_2 concentrations were below detection (anoxic) in all treatments and controls (fig. S1). Total adenylate [adenosine triphosphate (ATP) + adenosine diphosphate (ADP) + adenosine monophosphate (AMP)] concentrations, a proxy for microbial biomass (*36*), suggest that living biomass significantly accumulated (two-sided *t* test; $P = 0.002$) in the APM treatments ($n = 6$) relative to the controls ($n = 5$) at both 7 and 10 days (fig. S2). A principal components analysis of the gene expression profiles of the APM treatments ($n = 8$) and controls ($n = 5$) showed that microbial eukaryote gene expression in the presence of APM was significantly different from that of the controls (fig. S3). Moreover, microbial eukaryote gene expression at 7 and 10 days (under anoxia) with added APM was highly similar (fig. S3), motivating us to group these two time points together for comparison to the rest. The percentage of expressed genes by microbial eukaryotes was significantly higher (two-sided *t* test; $P = 0.005$) in the combined 7- and 10-day APM treatments ($n = 5$) than in the combined 7- and 10-day controls ($n = 3$) (Fig. 1A). In contrast, the percentages of expressed genes by bacteria and archaea were lower (two-sided *t* test; $P = 0.003$ and $P = 0.115$, respectively) in the treatments ($n = 5$) versus the controls ($n = 3$) at 7 and 10 days (Fig. 1A). Together, the higher total adenylate concentrations and greater percentage of gene expression by microbial eukaryotes in the AMP treatments versus the controls at 7 and 10 days suggest that APM stimulated the growth and activity of microbial eukaryotes under anoxia. To understand the cytological and physiological mechanisms underpinning the microbial eukaryotic response to APM, we investigated the functional genes overexpressed in APM treatments versus the controls.

To explore the number and identity of overexpressed genes in the anoxic 7- and 10-day APM treatments, we compared the microbial eukaryote metatranscriptomes in the presence of APM at 7 and 10 days ($n = 5$) against the grouped metatranscriptomes of the controls ($n = 5$) in a volcano plot (or overexpression) analysis (Fig. 1B). This analysis showed that APM was associated with a greater number of significantly (two-sided *t* test; $P < 0.05$) overexpressed genes ($n = 217$) compared to the number of significantly (two-sided *t* test; $P < 0.05$) overexpressed genes in the controls ($n = 2$) (Fig. 1B). More specifically, the presence of APM stimulated the expression of many key genes involved in phagocytosis (Fig. 1B). These overexpressed genes included genes encoding Rab guanosine triphosphatases (GTPases), SNAP receptor proteins, and vacuolar sorting proteins, all involved in phagosome formation (*37*, *38*), as well as genes encoding clathrin, coronin, and formin-like proteins, which are involved in cytoskeleton remodeling (*38*, *39*). These results suggest that the added APM promoted phagocytosis by protists under anoxia.

To identify the phylogenetic affinities of the microbial eukaryotes that exhibited the strongest response in the anoxic APM treatments

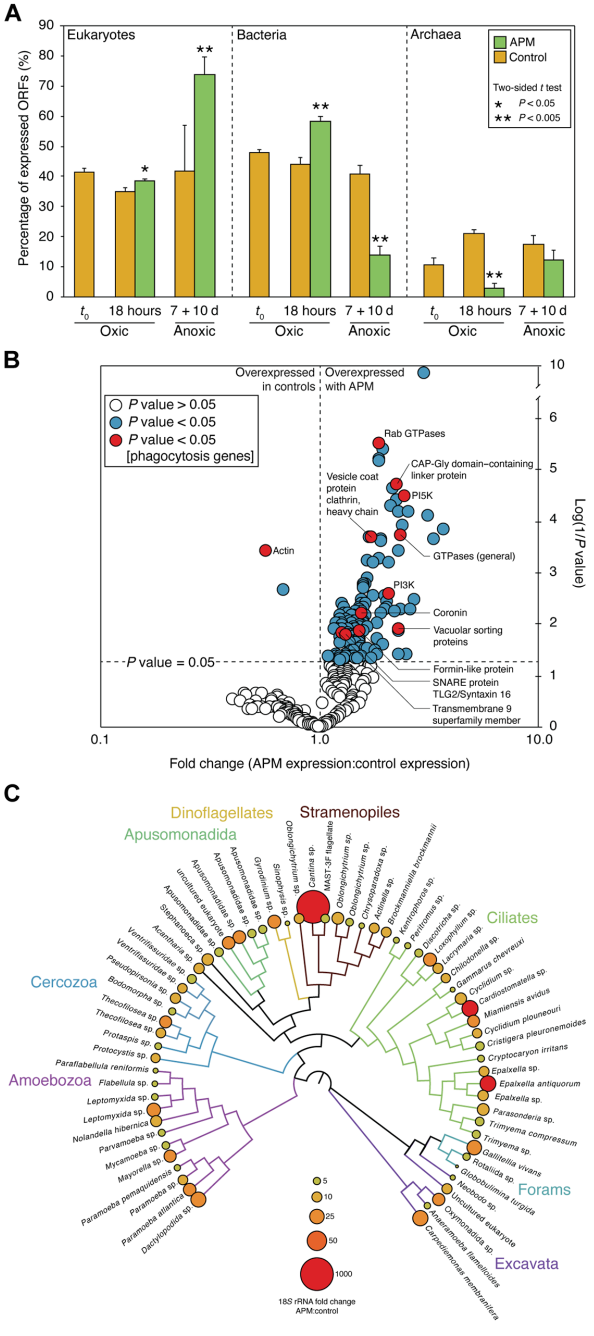

Fig. 1. The effect of added algal matter on eukaryote gene expression in anoxic sediment incubations. (**A**) The percentage of expressed open reading frames (ORFs) across the domains of life as a function of both time and the presence of APM. Asterisks denote statistically significant differences (two-sided *t* test; *P* values < 0.05; $n = 8$). Error bars represent SD. By 7 and 10 days, O_2 was below detection (fig. S1). (**B**) Significant overexpression of eukaryote genes in APM treatments ($n = 5$) relative to the controls ($n = 5$), with genes involved in phagocytosis labeled and marked in red. The vertical dashed line separates expressed genes that either increased or decreased in relative abundance with APM relative to the controls, while the horizontal dashed line represents the *P* value cutoff for determining statistical significance (two-sided *t* test; *P* values < 0.05). (**C**) Phylogenetic tree of 18*S* rRNA OTUs significantly (two-sided *t* test: $P < 0.05$; $n = 10$; fig. S5) overexpressed in the APM treatments, with bubbles proportional to the fold change in 18*S* rRNA expression between the treatments and controls. d, days; GTPases, guanosine triphosphatases.

at 7 and 10 days, we screened the metatranscriptomes of these two time points for expressed 18*S* ribosomal RNA (rRNA) genes (fig. S4). This screening resulted in the identification of 18*S* rRNA derived from 63 microbial eukaryote operational taxonomic units [OTUs; sharing 97% identity in 18*S* rRNA sequences, equivalent to species-level designation (*40*)] with significantly (two-sided *t* test; $P < 0.05$; $n = 8$) higher relative abundances in the presence of APM than in its absence (fig. S5). The closest relatives of the 18*S* rRNA revealed that most lineages with elevated 18*S* rRNA expression in the presence of APM belong to ancestrally eukaryovorous clades (*17*) with known Proterozoic (2500 to 539 Ma) origins, including the Amoebozoa (*8*), Cercozoa (*8*), and Foraminifera (*10*) (Fig. 1C). Overall, these results suggest that the added APM was directly phagocytosed by benthic eukaryovorous protists living under anoxia.

After confirming that the addition of APM stimulated phagocytosis in our treatments under anoxia, we explored the eukaryotic energy metabolism pathways that supported this behavior. Overexpression analysis identified multiple core anaerobic energy metabolism genes in eukaryotes (*41*) that were significantly (two-sided *t* test; $P < 0.05$) overexpressed with APM at 7 and 10 days ($n = 5$) compared to the controls ($n = 5$), including genes encoding alcohol dehydrogenase, citrate synthase, and phosphoenolpyruvate carboxykinase (fig. S6). These overexpressed genes are consistent with the fermentation of phagocytosed algal cells by anaerobic protists. However, a eukaryote copper-containing nitrite reductase (*nirK*) gene was also significantly (two-sided *t* test; $P < 0.05$) overexpressed in the APM treatment at 7 and 10 days, suggesting the capacity for some of the sampled anaerobic protists to conserve energy via anaerobic respiration using nitrite as a terminal electron acceptor. The ability of eukaryotes to survive, and even thrive, in anoxic environments via denitrification, including *nirK*-mediated nitrite reduction, has been shown to be a phylogenetically widespread trait than previously thought, present in ciliates (*42*), fungi (*43*), and foraminifera (*24*). Our results, therefore, suggest that the phagocytosis of algal prey under anoxia is energetically supported by both fermentation and anaerobic (nitrite) respiration by anaerobic eukaryovores, contrary to the view that such predatory behaviors require relatively high O_2 levels (*17*, *18*).

To assess whether the results of our APM experiments reflect the in situ activities of benthic protists living in the BUS, we compared the metatranscriptomes from our APM experiments ($n = 27$) to sediment and water column metatranscriptomes ($n = 13$) reported previously from the same sites of the same oceanographic region (*22*, *44*). This comparison showed that many of the eukaryote genes responsible for phagocytosis and anaerobic energy metabolism overexpressed in the APM treatments versus the controls were also expressed in the anoxic and sulfidic sediments of the BUS (Fig. 2). Moreover, the general expression of these genes was relatively lower in the oxic water column, with the notable exception of genes involved in glycolysis, which anaerobically precedes both respiration and fermentation (Fig. 2A). The relatively high expression of certain genes involved in phagocytosis—namely actin, myosin, and tubulin—in the water column is also expected, as phagocytosis demonstrably operates under both oxic and anoxic conditions (*19*). Overall, these gene expression patterns suggest that our anoxic APM treatments effectively promoted trophic interactions and anaerobic energy metabolisms exhibited by the protists living within the anoxic and sulfidic sediments of the BUS.

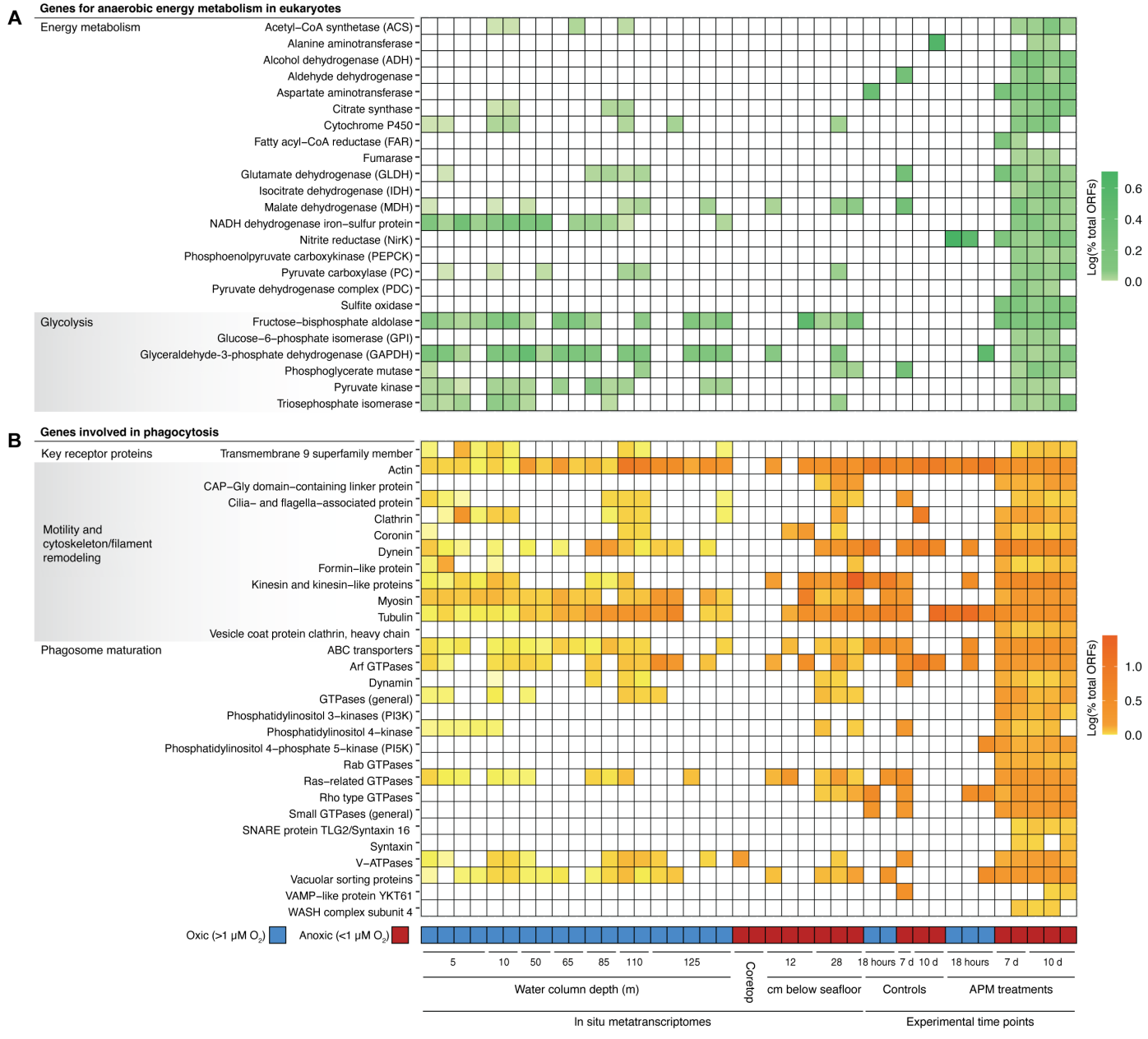

Fig. 2. Heatmap of expressed eukaryote genes involved in anaerobic energy metabolism and phagocytosis. (**A**) Genes involved in anaerobic energy metabolism in eukaryotes [collected from (*41*)] from in situ water and sediment samples from the BUS (left side; $n = 27$), as well as experimental time points (right; $n = 13$). (**B**) Genes involved in phagocytosis (*22*, *37*–*39*, *94*) across the same sampled metatranscriptomes. Heatmap coloring corresponds to the relative levels of gene expression (that is, percentage of total expressed genes), with darker colors indicating higher relative abundances. Blue and red squares at the bottom of the plot display the presence or absence of O_2 (above or below 1 μM O_2), respectively. NADH, reduced form of nicotinamide adenine dinucleotide; ATPases, adenosine triphosphatases; VAMP, vesicle-associated membrane protein; WASH, Wiskott–Aldrich syndrome protein and SCAR homologue.

Confirmed growth of anaerobic protists with high estimated growth efficiencies

The significant rise in protist gene expression with APM under anoxia (Fig. 1A) suggests increased activity and growth of anaerobic protists under these conditions. However, as metatranscriptomic data are only semiquantitative, increased gene expression by protists in our APM treatments could also be explained by decreased gene expression by bacteria and archaea. To confirm whether APM quantitatively stimulated the growth of anaerobic protists, we enumerated the calcium carbonate tests of benthic foraminifera in four different size ranges over the course of the experiment in both the treatments and controls (Fig. 3A). In two of the size ranges investigated—250 to 330 μm and 330 to 500 μm—we found that APM resulted in a higher number of foraminifera tests under anoxia at 7 and 10 days compared to the controls, especially for the genus *Bolivina* (Fig. 3A). These results demonstrate that the addition of

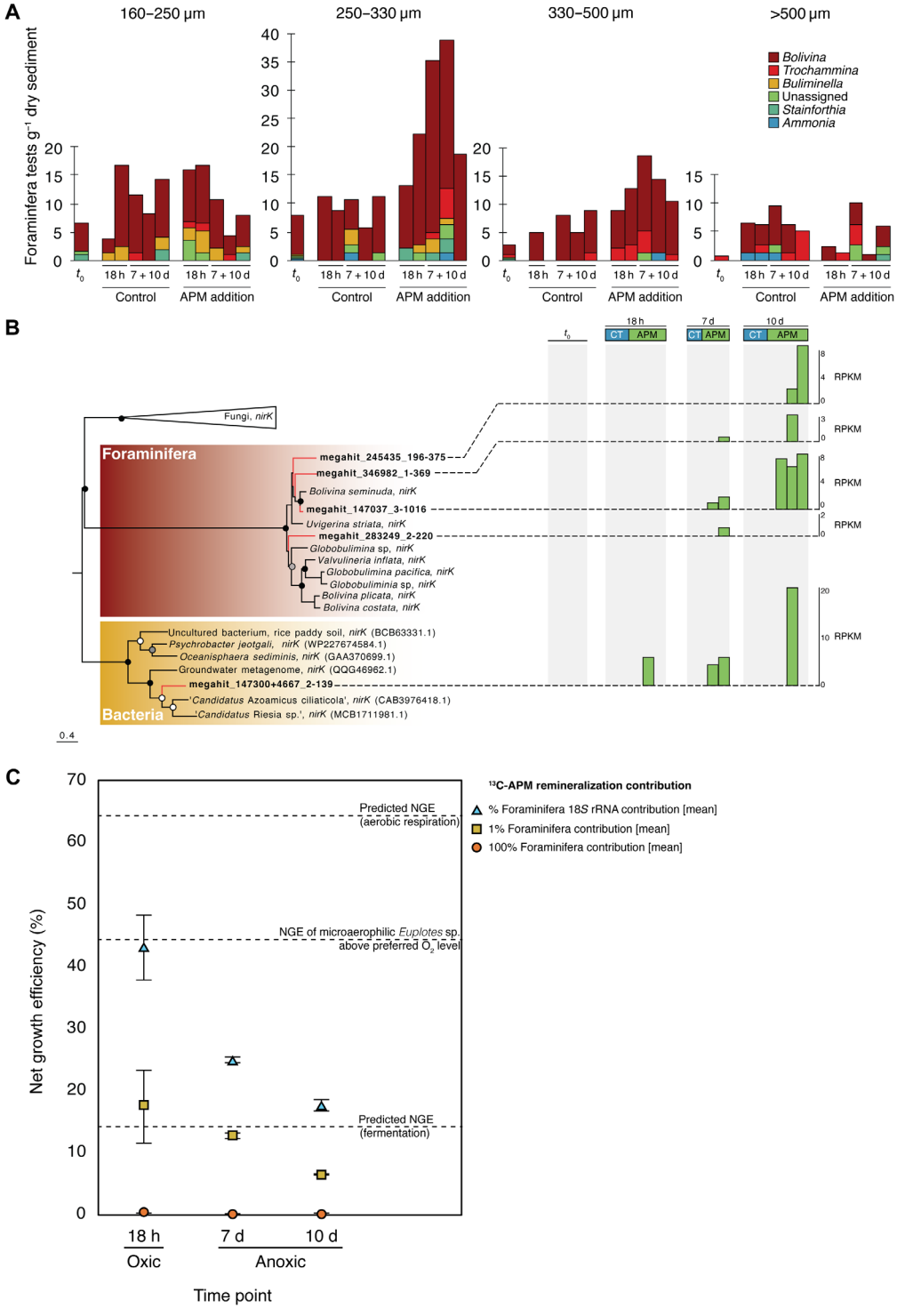

Fig. 3. Anaerobic growth and growth efficiencies of benthic foraminifera. (**A**) Concentration of foraminifera cells (tests) of different genera in the APM treatments and controls compared to the in situ state (t_0), according to four different size fractions. (**B**) Phylogenetic tree (PhyML) of foraminifera *nirK* transcripts, as well as a likely *nirK* expressed by *Candidatus* Azoamicus ciliaticola, a denitrifying endosymbiont of anaerobic ciliates (*23*). The panel to the right displays the expression of *nirK* ORFs in both the treatments and controls over time expressed as reads per kilobase mapped (RPKM). Note that the eukaryote *nirK* is only expressed in the presence of APM at 7 and 10 days under anoxia. (**C**) Net growth efficiency (NGE; see Materials and Methods) estimated for benthic foraminifera consuming ^{13}C-labeled APM in the presence and absence of O_2 and under three sets of assumptions regarding the fractional contribution of foraminifera to $^{13}CO_2$ production from ^{13}C-labeled APM. Error bars represent SE. Dashed lines represent calculated NGEs from (*28*) and (*45*). Note that the calculated NGEs for foraminifera growing under anoxia is higher than those calculated for fermenting (nonrespiring) protists under anoxia (*28*). h, hours. d, days.

APM increased the growth (that is, reproduction) of anaerobic foraminifera under anoxia, consistent with the 18*S* rRNA overexpression analysis indicating that several foraminifera lineages were stimulated by the addition of APM (Fig. 1C). It is well established that phagotrophic anaerobic foraminifera are active in anoxic marine sediments (*20*–*22*, *24*). These results suggest that the observed increase in eukaryote gene expression (Fig. 1A) and total adenylate concentrations (fig. S2) in the presence of APM is explained, at least in part, by the promoted growth of anaerobic protists by APM.

Given the demonstrable growth of foraminifera in the presence of APM, we combined our foraminifera growth rates with ^{13}C-APM remineralization rates (see Material and Methods) to estimate the efficiency of this growth. Net growth efficiency [NGE = (assimilated C)/(assimilated C + dissimilated C)] is theoretically estimated to be 64 and 14% for aerobic respiration and fermentation, respectively (*28*), and can be broadly estimated using our observed rates of foraminifera reproduction and ^{13}C-APM remineralization under different O_2 concentrations (fig. S7). Specifically, we used the growth and remineralization rates from the first 18 hours of the APM treatments when O_2 was detectable yet declining (from 124 μM O_2 at 0 hours to 2 to 31 μM O_2 at 18 hours), as well as the rates from 18 hours to 7 and 10 days when O_2 was predominantly undetectable (starting at ~22 hours) (fig. S1). Moreover, we surveyed three different scenarios to constrain the relative contribution of growing foraminifera to the observed $^{13}CO_2$ production (see Materials and Methods and Fig. 3C). The scenario that yields estimates closest to the predicted values assumes that the contribution of foraminifera to $^{13}CO_2$ production was proportional to the relative abundance of foraminifera 18*S* rRNA (of the total 16*S* and 18*S* rRNA) in our metatranscriptomes over the course of the experiment (see Materials and Methods). In this scenario, NGE in the presence of detectable O_2 is estimated to 43.0% (± 5.31)—less than the predicted 64% for aerobic growth (Fig. 3C). Meanwhile, the same scenario suggests that NGE in the absence of detectable O_2 is 24.9% (±0.52) and 17.7% (±0.83) at 7 and 10 days, respectively—both higher than the predicted 14% for fermentative growth.

The lower-than-expected NGE (43% versus 64%) for the first 18 hours of our APM treatments—if accurate—could potentially be explained by the cost of protection against O_2 toxicity if the growing benthic foraminifera were microaerophiles sensitive to elevated O_2 concentrations (fig. S1). A similarly low aerobic NGE (44.0%) was estimated for the microaerophilic ciliate *Euplotes* sp. when exposed to O_2 levels exceeding its preferred ~5% of atmospheric saturation (where its NGE was 60.5%) (*45*). At the time of sampling, the O_2 concentration in the water column immediately overlying the sampled sediments was 24.3 μM O_2 (8.79% of atmospheric saturation at 11°C and 35 S) (fig. S8), so the relatively high O_2 concentrations (124 μM O_2 or 44% of atmospheric saturation at 10°C and 35 S) at the beginning of our experiments could have exceeded the preferred O_2 concentrations of the growing benthic foraminifera if they were microaerophiles.

With respect to the 7- and 10-day intervals (starting at 18 hours), the higher-than-predicted NGEs can potentially be explained by aerobic respiration—for example, during the first few hours of detectable O_2 (fig. S1)—or by anaerobic respiration. Numerous benthic foraminifera respire NO_3^- in addition to O_2 (*24*), with metabolic scaling evidence supporting NO_3^- as the preferred electron acceptor (*21*). The complete or partial reduction of NO_3^- to N_2 (denitrification) by benthic foraminifera is accomplished via enzymes encoded in their own genomes (rather than in the genomes of intracellular bacteria) (*46*). We identified several foraminifera *nirK* genes expressed in the presence of APM, although no foraminifera *nirK* expression was detected in the controls or in the in situ water and sediment samples (Figs. 2A and 3B). These expressed foraminifera *nirK* genes branch most closely to members of the genus *Bolivina* (Fig. 3B), consistent with increasing *Bolivina* tests in the presence of APM (Fig. 3A).Together, these results suggest that the addition of APM promoted the growth of NO_2^--respiring foraminifera (including members of the genus *Bolivina*), potentially explaining the higher-than-expected NGEs under anoxia (Fig. 3C), as NO_2^- reduction (a form of anaerobic respiration) conserves more energy than substrate level phosphorylation and fermentation per unit substrate (*28*).

In addition to foraminifera, we identified *nirK* expression by "*Candidatus* Azoamicus ciliaticola" (Fig. 3B), a denitrifying bacterial endosymbiont of anaerobic ciliates (*23*). Similar to the *nirK* expression by foraminifera, the *nirK* expression by "*Ca.* A. ciliaticola" only occurred in the presence of APM (Fig. 3B). Furthermore, the APM-associated overexpression of 18*S* rRNA by three members of the class Plagiopylea—the only known class of ciliates known to host *Ca.* A. ciliaticola (*23*)—further bolsters evidence for this symbiosis in our treatments (Fig. 1C). Collectively, these results suggest that APM stimulated denitrification in both foraminifera and the bacterial endosymbionts of anaerobic ciliates, demonstrating the need for improved transcriptome sampling of anaerobic protists and their symbionts to resolve the nature and distribution of denitrification across the eukaryote tree. Now, within the Foraminifera, denitrification is confined to the order Rotaliida, which is estimated to have originated by the Permian Period (299 to 252 Ma), hundreds of millions of years after the Rise of Algae (*24*). While increased metatranscriptome sampling is needed to test whether eukaryote denitrification extends back to the Precambrian, there is now no available evidence for *nirK*-mediated denitrification in the Foraminifera in the Neoproterozoic Era. Nevertheless, our results suggest that the NGEs of anaerobically respiring foraminifera are greater than those of fermentative protists and that denitrification by phagotrophic foraminifera may correspondingly increase the carbon, energy, and nutrient flux to eukaryote predators (including animals) in the anaerobic benthos of the BUS.

DISCUSSION

Eukaryote predation under anoxia in the Neoproterozoic Era

Our results demonstrate that algal biomass stimulates the growth and activity of phagotrophic anaerobic protists living just beneath the seafloor of the O_2-depleted BUS. By extension, we predict that the proposed Rise of Algae (*5*) would have similarly promoted the ecology of phagotrophic lineages living in the benthos of the Neoproterozoic Era, before the establishment of modern marine O_2 levels (*3*). Three of the clades with overexpressed 18*S* rRNA in our APM treatments (Fig. 1C) have body fossil records extending back to the Neoproterozoic Era: the Amoebozoa (~770 to 742 Ma) (*8*, *9*), the Cercozoa (~770 to 742 Ma) (*8*), and potentially the Foraminifera (~716 to 635 Ma) (*10*, *47*). While the remaining clades with overexpressed 18*S* rRNA in the presence of APM (Fig. 1C) apparently lack clear Proterozoic body fossils—potentially due to taphonomic biases (*48*)—numerous molecular clock estimates infer their presence by the Neoproterozoic Era (*49*–*51*).

While modern phagotrophic clades likely extend back to the Neoproterozoic Era (*9*, *17*, *52*), it remains unclear whether the genes mediating phagocytosis then were the same genes mediating phagocytosis today (given the possibility of gene replacement and loss) (*53*). For our purposes, we used the expression of key genes now involved in phagocytosis (Fig. 2B) to infer whether phagocytosis (as a process) was occurring in our water, sediment, and incubation samples and was therefore permitted by the associated redox conditions (Figs. 1B and 2). In our sediment incubations, APM stimulated phagocytosis (Figs. 1B and 2) and promoted phagocytic clades (Figs. 1C and 3A) under anoxia, suggesting that phagotrophs internalized the APM as a carbon and energy source while reproducing. On the basis of these results, we propose that exported APM would have similarly promoted phagotrophic protists living in anoxic marine sediments in the Neoproterozoic, even if different genes were involved in phagocytosis then. However, this interpretation also requires that phagotrophic crown-eukaryotes in the Neoproterozoic had the genes necessary for metabolizing anaerobically.

The origins of anaerobic energy metabolism in eukaryotes are controversial and unsettled (*54*, *55*). Specifically, while LECA is universally thought to have respired O_2, it is debated whether LECA was an obligate or facultative aerobe (*56*). In the latter scenario, enzymes for anaerobic energy metabolism were acquired during eukaryogenesis before LECA, either from the alphaproteobacterial ancestor of mitochondria via endosymbiosis (*41*, *54*) and/or from other bacterial donors via lateral gene transfer (LGT) (*55*, *57*). If LECA—which almost certainly emerged before the Neoproterozoic Era (*1*)—was a facultative aerobe, then crown-eukaryote lineages in the Neoproterozoic would have already had enzymes necessary for metabolizing anaerobically under anoxia. The alternative (LECA was an obligate aerobe) is difficult to reconcile with the low and dynamic marine O_2 concentrations reconstructed for the mid-Proterozoic (*56*), even if eukaryogenesis took place in cyanobacterial mats (*58*), which are ephemeral environments that generally—but not universally (*59*)—exhibit diurnal cycles of anoxia (especially under anoxic water columns) (*60*). Despite uncertainties in the origin of anaerobic energy metabolism in eukaryotes, the most parsimonious interpretation is that enzymes for anaerobiosis had already been acquired (whether by endosymbiosis and vertical inheritance and/or by LGT) by crown-eukaryotes before the Neoproterozoic (*41*, *56*).

While our model system—the BUS—exhibited bottom-water O_2 concentrations approaching those reconstructed for the Neoproterozoic surface ocean at the time of sampling (fig. S8) (*3*), it is importantly not a "Neoproterozoic ocean analog." Abiotic features of the BUS like seawater temperature, PO_4^{3-} availability, and carbonate chemistry (associated with high organic carbon remineralization rates) are all definitively modern and likely uncharacteristic of the global Neoproterozoic ocean (*61*–*63*). Ecologically, primary productivity at the BUS greatly exceeds estimates for the Neoproterozoic—<10% of modern global levels (*64*)—and is dominated by phototrophic clades (namely dinoflagellates and diatoms) that only became ecological pervasive in the Mesozoic Era (252 to 66 Ma) (*65*). Our APM was sourced from a culture *Chaetoceros socialis* (Materials and Methods), a planktonic diatom representative of primary producers from the BUS (*66*), suggesting that our sediment incubations captured in situ (rather than artificial) ecological interactions in the BUS (Fig. 2). Despite these discrepancies between the BUS and the Neoproterozoic ocean, which are unavoidable, our results nevertheless demonstrate that anoxia permits the consumption of exported APM by phagocytic eukaryote clades present in the Neoproterozoic. That said, future studies investigating the benthic processing of APM derived from planktonic chlorophytes and rhodophytes, as well as planktonic cyanobacteria, would provide additional constraints necessary for reconstructing the trophic ecology of the Neoproterozoic benthos.

The Rise of Algae and the evolution of the microbial loop

The Rise of Algae was originally constrained temporally to ~659 to 645 Ma in the interval between the Sturtian and Marinoan "snowball Earth" glaciations of the Cryogenian Period (720 to 635 Ma) (*5*). This chronology was based primarily on the first appearance of extractable stigmastane—regular C_{29} steranes associated with green algae—combined with a shift to higher sterane to hopane ratios (*5*). The oldest extractable saturated steranes in the rock record date back to ~820 to 720 Ma in the Tonian Period (1000 to 720 Ma) [although see claims for kerogen-bound steranes ~1400 Ma (*67*)] and are almost exclusively dominated by C_{27} steranes (cholestane). While these oldest extractable steranes were initially interpreted as the remains of nonphotosynthetic protists (*5*), they (along with co-occurring aromatic steroids) are now interpreted as the probable remains of red algae, suggesting an increase in the relative abundance of red algae in the Tonian Period before the Sturtian glaciation and the subsequent "rise of chlorophytes" (*2*, *6*). In the Ediacaran Period (635 to 539 Ma), the high relative abundance of stigmastane among saturated steranes suggests that green algae were established as the dominant eukaryote primary producers at this time—a pattern extending into the Paleozoic Era (539 to 419 Ma) (*2*, *6*). With respect to the body fossil record, the Tonian "rise of rhodophytes" (*2*) broadly correlates with the oldest evidence for the Amoebozoa and Cercozoa (~770 to 742 Ma) (*8*), while the Ediacaran establishment of abundant green algae broadly correlates with the oldest unequivocal evidence for crown-group Metazoa ~570 Ma (*16*).

Both body fossils and molecular clock estimates suggest that crown-Archaeplastida had emerged by the Mesoproterozoic Era (1600 to 1000 Ma) (*4*, *68*). As a result, the Rise of Algae is usually interpreted as representing an environmentally or ecologically driven shift in the relative abundance of preexisting Archaeplastida lineages (*5*, *6*, *15*, *69*). How members of the Rhodophyta and then Chloroplastida shifted to higher relative abundances in the mid-to-late Neoproterozoic Era, however, remains unclear. Originally, when the Rise of Algae was constrained to the Sturtian-Marinoan interglacial, enhanced phosphorus delivery to a nutrient-poor ocean in the wake of the Sturtian glaciation was proposed as the proximate environmental driver (*5*, *15*), as cyanobacteria (with their higher surface area to volume ratios) generally outcompete larger algae under strong phosphorus limitation (*70*). During this bloom of elevated marine productivity, it was proposed that the preferential grazing of bacteria-eating (or bacterivorous) protists on cyanobacteria actively encouraged the growth of larger algae by limiting cyanobacterial population densities and re-releasing limiting nutrients back into the surface ocean (*5*, *11*, *15*). This self-sustaining proliferation of algae, in turn, promoted the expansion of eukaryovorous protists, thereby driving the evolution of increasingly large cell sizes, the number of taxa occupying higher trophic levels, and novel predator-prey interactions (*5*, *11*, *15*). The later recognition that red algae (*6*)—and sterol-synthesizing crown-group eukaryotes more generally (*2*)—likely increased in global abundance in the Tonian Period challenges the idea that postglacial weathering in the Cryogenian

Period served as the immediate environmental cause of the Rise of Algae (or at least the rise of rhodophytes). Alternate (and complimentary) mechanisms for the Tonian expansion of red algae include increasing marine oxygen (*71*) and nitrate (*72*) availability, as well as an increase in the effectiveness of bacterivory (*73*), perhaps explained by the refinement or acquisition of phagocytosis more broadly across the eukaryote tree (*7*, *39*, *53*). Alternatively, crown-Archaeplastida may have already been abundant in the Mesoproterozoic ocean, with preservational artifacts explaining the apparent pre-Tonian absence of extractable steranes (*67*, *68*, *74*). Regardless of the exact timing and trigger(s) for the initial proliferation of marine Archaeplastida, the export of algal cells to the Proterozoic seafloor would have likely permitted the growth and activity of benthic eukaryovorous protists living under anoxia, as demonstrated here.

Increased oxygen and nutrient availability and the associated expansion of planktonic algae in the Neoproterozoic ocean are predicted to have augmented the export of surface-derived APM to marine sediments (*5*, *15*). This exported APM is thought to have been a critical and direct food source to the earliest suspension-feeding benthic metazoans (*5*, *15*), which potentially entered the body fossil record as early as ~571 to 560 Ma (e.g., *Thectardis* from the "Avalon" assemblage) (*75*, *76*) and the lipid biomarker record by ~635 Ma (i.e., 24-isopropylcholestanes interpreted as the remains of demosponges) (*12*). However, our results here demonstrate that the efficient export of APM to marine sediments would have similarly stimulated the growth and activity of benthic anaerobic protists, which would have rerouted carbon, energy, and nutrient fluxes to burgeoning animal ecosystems during the mid-to-late Neoproterozoic Era (Fig. 4). Anaerobic protists living just beneath the sediment-water interface, or in the anoxic layers of benthic microbial mats, could have been processed by Ediacaran animals like *Kimberella*, which grazed on the surfaces of microbial mats (*77*), or *Dickinsonia*, which consumed externally digested mat surfaces via its lower epithelium (*78*). Alternatively, if these Ediacaran feeding modes were too spatially decoupled from anaerobic protists—which presumably lived just below the uppermost oxic layers of microbial mats and marine sediments—abundant benthic anaerobic protists potentially established the interstitial carbon and nutrient reservoirs necessary for the eventual evolution of metazoan meiofauna closer to the Ediacaran-Cambrian boundary (*79*). Furthermore, while our experiments were primarily conducted under anoxia, we predict that exported APM would have similarly promoted the growth and activity of aerobic, epibenthic phagotrophs more probably accessible to Ediacaran surface grazers. Overall, the APM-stimulated growth of anaerobic phagotrophs in the Neoproterozoic benthos would have established key linkages between the benthic microbial loop and nascent animal food chains (Fig. 4).

Overall, the Neoproterozoic Rise of Algae—when marine eukaryote primary producers began increasing in global abundance ~820 to 635 Ma—is predicted to have promoted the growth and ecological expansion of eukaryovorous protists (*5*, *15*), which confidently entered the body fossil record around this time (*8*, *9*). So far, the predation of phagotrophic protists on marine algae and other microbial eukaryotes has largely been thought to have been exclusive, or nearly exclusive, to the Neoproterozoic marine water column (*17*, *18*), where dissolved oxygen concentrations were predominantly "suboxic" or "severely hypoxic" by modern oceanographic standards (<8% of present atmospheric saturation, $T = 11°C$, $S = 35$) (*3*). We demonstrate, however, that the input of algal cells to sediments collected at

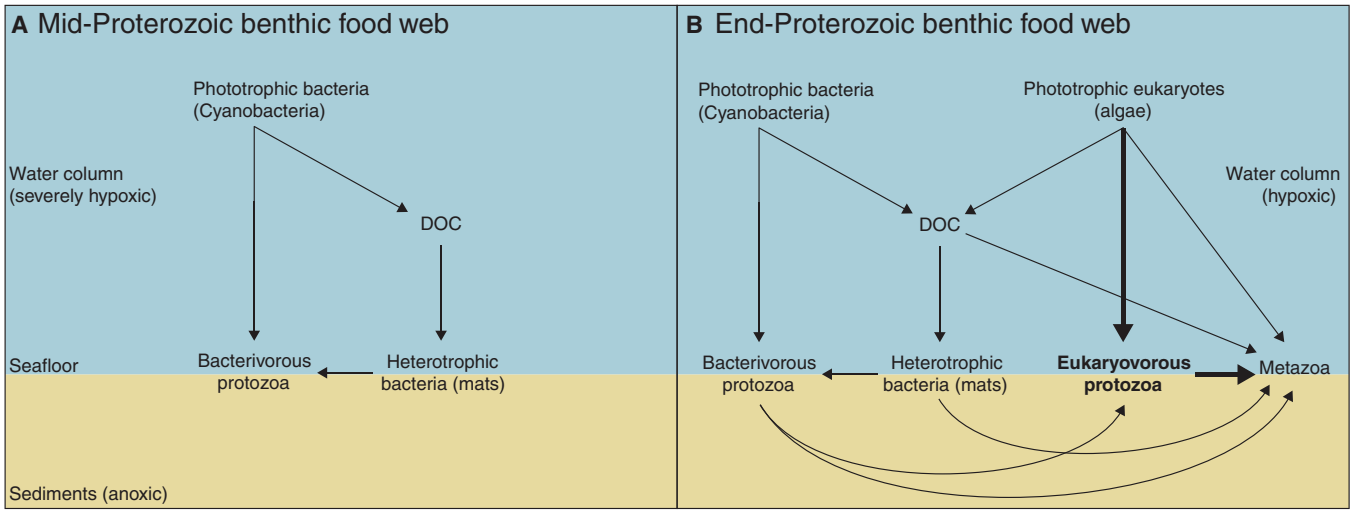

Fig. 4. The evolution of benthic food webs from the mid- to late-Proterozoic Eon. (**A**) Simplified (nonexhaustive) schematic of the microbial loop before the primary acquisition of plastids yet after the origin of phagotrophy (the eukaryote feeding mode in which microbial prey are internalized via phagocytosis). Marine surface waters in equilibrium with the atmosphere at this time likely had O_2 concentrations corresponding to 1 to 10% of modern atmospheric saturation and were therefore severely hypoxic (4.8 to 22 μM O_2) by modern oceanographic standards (*3*). The earliest phagotrophs were probably (bacterivorous) protozoa that phagocytosed bacteria (and archaea) from both the water column and benthos, before the origin of eukaryote-on-eukaryote predation (eukaryovory) (*95*). (**B**) Simplified schematic of the microbial loop toward the end of the Proterozoic Eon, after the permanent establishment of abundant eukaryote primary producers. By this time, the O_2 content of shallow marine environments was likely increasing but was still "hypoxic" (22 to 63 μM O_2) by modern standards (*3*). The bold arrows indicate the consumption of exported APM by benthic eukaryovorous protozoa (as demonstrated by this study), followed by the consumption of these protozoa by the earliest benthic animals (metazoans). By the end-Proterozoic, metazoans likely consumed dissolved organic carbon (DOC) via osmotrophy (*75*, *96*), mat-forming bacteria and associated protozoa via both surface grazing (*77*) and external digestion (*78*), planktonic microbes via suspension feeding (*76*), and benthic microbes via infaunal deposit feeding (*76*). Schematic inspired by figure 1 from (*25*).

the sediment-water interface of a modern oxygen-depleted upwelling zone (with bottom water oxygen levels ~9% of present atmospheric saturation, T = 11°C, S = 35) stimulates the growth and activity of anaerobic phagotrophs under anoxia. Specifically, we observed the overexpression of key genes involved in both phagocytosis and anaerobic energy metabolism in metatranscriptomes collected from anoxic sediment incubations with added ^{13}C-labeled algal cells. We additionally observed the growth (reproduction) of benthic foraminifera under anoxia with higher-than-expected net growth efficiencies, potentially explained by the expression of a eukaryote nitrite reduction pathway. Together, our results suggest that the export of algal-derived particulate matter to the seafloor during the Rise of Algae would have stimulated the growth and activity of benthic phagotrophs living under anoxia. This promotion of eukaryote biomass in the Neoproterozoic benthos would have redirected carbon, energy, and nutrients away from bacteria and archaea and toward newly evolving metazoan trophic levels, facilitating the evolution of modern food webs.

MATERIALS AND METHODS

Sampling and APM experimental setup

During *F/S* Meteor Expedition "EreBUS," multicoring was used to obtain a sediment core on the Namibian continental shelf (18.0 S, 11.3 E) from a water depth of 125 m, as described previously (*22*). This coring yielded a 30-cm-long core (with an intact sediment-water interface) that was immediately placed in a 4°C cold room. Within 24 hours of retrieval, sediments from the core top (the uppermost 5 mm) were collected and incubated in duplicate for 18 hours, 7 days, and 10 days with either ^{13}C-labeled APM or no added APM as a control. Specifically, 2 g of core top sediment was added to 20-ml glass flasks, which were then filled with bottom-water seawater (S = 35; collected from the multicorer), leaving no headspace. The flasks were then crimp-sealed gas-tight using gray butyl rubber stoppers and were incubated horizontally in the dark at 10°C. Each flask was equipped with two O_2 sensor spots (PreSens, Regensburg) situated both above and below the sediment. A Fibox was used to continuously measure O_2 on both spots throughout the incubations, as described previously (*22*). At each time point, duplicate flasks were frozen at −20°C in plastic 50-ml Falcon tubes (since glass flasks can crack upon thawing before RNA extraction). By freezing the crimp-sealed glass flasks immediately at each time point, the flasks did not need to be reopened for sampling, which would have exposed the anoxic incubations to O_2 during intermediate sampling points. Therefore, all APM and control incubations remained anoxic after approximately 20 hours until being frozen at either 7 or 10 days.

APM was produced using a culture of the planktonic diatom *C. socialis* (Norwegian Culture Collection strain K1676) grown using L1 growth medium (*80*) at 22°C for 7 days while exposed to natural day-night cycles. The culture was grown with 2 mM 99% ^{13}C-labeled sodium bicarbonate, which the diatoms used as a carbon source. After 7 days, the cultures exhibited turbidity and were filtered through a 0.2-μm filter to remove any low molecular weight organic matter and to retain algal cells. The algal particulate phase was then removed from the filter surface using a sterile spatula and was stored at 4°C until being added to the incubations. The percent ^{13}C enrichment of the APM was determined previously to be >50% (*22*). The APM was added at a final concentration of 200 μg ^{13}C-labeled APM per gram sediment. This concentration corresponds to approximately 1 to 3% of the in situ sedimentary organic matter content (*22*). Since sinking *C. socialis* biomass is a major contributor to the organic carbon content of Namibian shelf sediments (*31*), the added APM serves as an appropriate proxy for tracking the predation of exported algae present in BUS surface waters by eukaryovorous protists living in the underlying sediments.

Total adenylate measurements

Total adenylate (ATP + ADP + AMP) was measured as a proxy for total biomass, as described previously (*36*). Briefly, 0.5 g of sample was mixed with 1 ml of sterile MilliQ water, incubated at 99°C for 10 min, and centrifuged for 2 min at 13,000 rpm. The total adenylate of the supernatant was measured using a luminometer with the A3 assay according to the manufacturer's instructions (A3 Lucipac, Kikkoman). Relative light units were converted to nanomolar total adenylate, as described previously (*36*).

RNA extraction and metatranscriptome library preparation

RNA extraction followed the same protocol as previously described (*22*, *44*). To reduce DNA contamination, all RNA samples were extracted in a high efficiency particulate air (HEPA)-filtered laminar flow hood dedicated only for RNA work (no DNA allowed inside) that also contains dedicated RNA pipettors used exclusively inside the hood with RNA samples. The pipettors were also autoclaved to remove contaminating RNA before every extraction. All surfaces were treated with RNAse-Zap before extractions and exposed to ultraviolet light for 30 min before and after each extraction.

RNA was extracted from duplicate incubations for each treatment, at each time point, serving as biological replicates. For the 7-day control samples, insufficient RNA was extracted for metatranscriptome library prep, and therefore the RNA from the duplicate incubations was pooled to create a single metatranscriptome. For the 18-hour and 10-day time points, technical replicates were performed from one of the biological replicates resulting in three total replicates (two biological replicates + one technical replicate), for controls and APM treatments, respectively.

The extracted RNA was used for deoxyribonuclease treatment, synthesis of cDNA, and metatranscriptome library construction, using the Trio RNA-Seq kit protocol (NuGEN Technologies) and procedures, as described previously (*22*, *44*). Metatranscriptome libraries were sequenced using paired-end 300 high-output kits on the Illumina MiniSeq. Metatranscriptome libraries were sequenced to an average depth of 7.1 million (SD = 1.3 million) as paired-end reads that were obtained after Illumina sequencing, which could be assembled de novo into an average of 17,367 (SD = 8263) contigs per library. Quality control, de novo assembly, and open reading frame (ORF) searches were performed as described previously (*44*).

Metatranscriptome annotation

Transcripts from the metatranscriptomes that encoded ORFs were searched for similarity using BLASTp against an aggregate database ("MetaProt") (*22*) containing predicted proteins from all protist, fungal, bacterial, and archaeal genomes and metagenome-assembled genomes (MAGs) in the Joint Genome Institute (JGI) and National Center for Biotechnology Information (NCBI) databases using double index alignment of next-generation sequencing data (DIAMOND) (*81*). This database included all ORFs from the >700 transcriptomes of microbial eukaryotes from the Marine Microbial Eukaryote Transcriptome Sequencing Project (MMETSP) (*82*). The custom

MetaProt database that we used for this study has been published previously (*22*, *44*) and is available as a single 32-GB amino acid FASTA file on the Ludwig Maximilian University (LMU) Open Data website (doi.org/10.5282/ubm/data.183). For functional annotations of the genes in the MetaProt database, we used the existing annotations provided by the respective databases (NCBI, JGI, and RefSeq). In the cases when no functional annotation was provided, such as in the case of the MMETSP dataset, we annotated the data via BLASTp against SwissProt. We assigned ORFs as being derived from either protists, bacteria, archaea, or fungi, based on a minimum bit score of 50, minimum amino acid similarity of 60, and an alignment length of 15 residues. We assigned ORFs as being derived from one of these four major groups if they met two criteria: (i) significant similarity above this threshold to a predicted protein from a previously sequenced transcriptome or genome from this group; and (ii) the top ORF was the best BLAST hit in the MetaProt database. Protist expressed ORFs in the metatranscriptomes were assigned to general categories of cellular function, via BLASTp searches against the Eukaryotic database of Orthologous Genes (KOG) (*83*). Contamination in the metatranscriptomes was determined from sequencing lab blanks and consistently consisted of human- and soil-associated bacteria such as *Streptococcus*, *Acinetobacter*, *Staphylococcus*, *Rhizobium*, *Ralstonia*, and *Burkholderia*. All ORFs deriving from a known contaminant organism, including those known as common kit contaminants (*84*), were removed before analysis.

18*S* rRNA annotation and analysis in metatranscriptomes

Metatranscriptomes were searched for 18*S* rRNA using SqueezeMeta (*85*), as described previously (*44*), which resulted in 5521 putative 18*S* rRNA contigs with an average length of 309 (SD = 97) bp. Putative 18*S* rRNA contigs identified with SqueezeMeta were searched for significant similarity to high-quality full-length 18*S* rRNA gene OTU sequences (clustered at 97% identity) in the Silva database version 138 (*86*). Those 18*S* rRNA contigs from SqueezeMeta that did not have a top hit to a named protist in Silva were further searched against the protist 18*S* rRNA gene databases PR2 (*87*) and EukRef (*88*). After this curation, 815 assembled contigs could be reliably identified as protist 18*S* rRNA sequences. Because the protist 18*S* rRNA contigs obtained were relatively short, they could potentially be different regions of the 18*S* rRNA from the same protist taxon, particularly if multiple short fragments all have the same 18*S* rRNA gene sequence as the most identical hit in the databases. Therefore, for those 18*S* rRNA contigs that had the same top hit with BLASTn, they were assumed to derive from the same (or highly similar) taxa, and their relative abundance was summed across samples. OTUs were defined using this reference-based approach, where 18*S* rRNA contigs (and their relative abundances) were grouped according to their closest relatives in the respective databases. In other words, 18*S* rRNA contigs that had top hits to different database sequences were considered different OTUs. This approach is reasonable, because the database used to compare against consisted only of preclustered OTU sequences that are all 3% different from one another (*86*). The relative abundance of the 18*S* rRNA was calculated as reads per kilobase mapped (RPKM) values provided in OTU table format from SqueezeMeta which allowed for statistical analyses of taxon overexpression in the APM treatments and visualization with volcano plots (see below).

Phylogenetic analysis

The full-length 18*S* rRNA genes from the closest relatives of metatranscriptome partial 18*S* rRNAs were aligned using multiple sequence comparison by log-expectation (MUSCLE) (*89*) in SeaView (*90*), followed by phylogenetic analysis with PhyML (*91*). Potential eukaryotic *nirK* ORFs were identified by first annotating all ORFs that had a top hit to a protist transcriptome or genome in our MetaProt database (see above). All potential protist ORFs were then searched via BLASTp against the KOG (*83*), which we amended with all eukaryote *nirK* sequences that we could obtain and verify from public databases. This included fungal, ciliate, and foraminifera *nirK* sequences that have been published in recent genomic and transcriptomic studies (*24*, *46*). The database also included the *nirK* of the recently discovered "*Candidatus* Azoamicus ciliaticola," a denitrifying endosymbiont of anaerobic ciliates belonging to the class Plagiopylea (*23*). Those ORFs having significant similarity to a eukaryote *nirK* were aligned using MUSCLE (*89*) in SeaView (*90*). Phylogenetic analysis of the resulting amino acid alignments of the predicted NirK proteins was conducted with PhyML (*91*) with BLOSUM62 as the evolutionary model and 100 bootstrap replicates.

Normalizing gene expression

The relative abundance of ORFs in metatranscriptomes was normalized to the percent of total ORFs and then log-transformed to account for variation in technical variability previously observed with this method (*22*, *44*). For volcano plot or overexpression analyses (e.g., Fig. 1B), we grouped the protist ORFs in metatranscriptomes from the 7- and 10-day incubations from the APM treatments ($n = 5$) and the 18-hour, 7-day, and 10-day controls ($n = 3$). The grouping of 7- and 10-day samples was based on the fact that the 7- and 10-day incubations were anoxic and shared similar expression profiles in principal components analysis (fig. S3). Using these groupings, normalized ORF expression values were averaged across the grouped control and APM replicates, respectively. Then, the expression ratio of APM:control was used to determine the fold change for over- or underexpression. To calculate a ratio for ORFs that did not have any detection in either the control or APM treatments, the detection limit value of 0.1 was added to all averages (because a zero ratio cannot be used to calculate an average). In this manner, ORFs with a fold change of >1 have overexpression in the APM treatment, and ORFs with a fold change of <1 have underexpression with APM. Statistical significance of ORF fold change in expression between controls and APM treatments was determined by a two-sided *t* test (P value < 0.05). Volcano plots were used to visualize the relationship between over- and underexpression by plotting the P value of an ORF against its corresponding fold change. The same procedure was used to determine over- and underexpression of 18*S* rRNA by specific protist taxa that resulted in the identification of 63 protist OTUs that were significantly (two-sided *t* test; P value < 0.05) enriched in relative abundance in the presence of APM and anoxia (Fig. 1C).

Measuring remineralized ^{13}C from ^{13}C-labeled APM

To quantify the remineralization of the added ^{13}C-labeled APM, we determined the relative amount of $^{13}CO_2$ produced using gas chromatography–mass spectrometry (GC-MS). Specifically, 0.2 g of incubation material was added to 20-ml crimp-sealed glass flasks and heated to 60°C for 5 min in a headspace sampler. An autosampler was used to sample 1 ml of headspace gas, which was then injected into to a gas chromatograph with a quadrupole mass spectrometer as the detector (GCMS-QP2020 NX, Shimadzu) using N_2 as the carrier gas. The GC-MS setup is calibrated for trace gas analysis (H_2,

CO, CO_2, and CH_4) by means of a preseparation column [U-Bond, 0.32 mm inner diameter (ID), 10-μm Film, 30 m] to separate larger molecules and a second column (Carboxen-1010 Plot, 0.32 mm ID, 15-μm Film, 30 m) for separating trace gasses. The elution time for CO_2 in this particular setup (6.1 min) was determined by comparison to a CO_2 standard (99.999% Linde Gas). The percentage of remineralized carbon from the labeled APM was calculated by comparing ^{13}C-labeled CO_2 [mass/charge ratio (m/z) = 45] relative to unlabeled CO_2 (m/z = 44) via integration of peak areas in the GC-QMS trace corresponding to either m/z = 45 or m/z = 44.

Size separation and counting of foraminifera

To count benthic foraminifera, 1 g of incubation slurry was sieved through a plastic serial filtration tower containing four filter meshes with the following sizes (in order): 500, 330, 250, and 160 μm. The sample was added to the top filter mesh (500 μm) and then washed 10 times with 500 ml of sterile MilliQ water with gentle shaking to spread the sample evenly on the mesh surface and to allow smaller particles to move through the mesh. After washing, the four different filter meshes were removed from the tower and dried on paper towels overnight. The dried contents of each mesh were then transferred to a sterile plastic petri dish, and foraminifera were identified and counted using a dissection microscope. We acknowledge that our enumeration is only able to identify foraminifera tests that are larger than 160 μm, and therefore, it is possible that some smaller foraminifera tests escaped our quantification. Therefore, our results should be viewed as an underestimate of the total foraminifera biomass.

Calculating net growth efficiencies of anaerobic foraminifera in the presence of APM

Fenchel and Finlay (*28*) define NGE as the fraction of carbon that is assimilated out of the total carbon that is assimilated and dissimilated during growth [NGE = (assimilated C)/(assimilated C + dissimilated C)]. Therefore, the NGE of the foraminifera that grew in our APM treatments can be estimated using our observed foraminifera growth and ^{13}C remineralization rates. Specifically, we solved for NGE (in terms of biovolume) using the following equation, where μ is the foraminifera growth rate constant, V_{foram} is foraminifera biovolume, U is the measured $^{13}CO_2$ production rate, and V_{AMP} is the *C. socialis* biovolume

$$\text{NGE} = \frac{[\mu \times V_{\text{foram}}]}{[\mu \times V_{\text{foram}}] + [U \times V_{\text{AMP}}]}$$

Foraminifera growth rate constants were estimated using the linear regression of the logarithm of foraminifera test counts during different time intervals of growth (e.g., 18 hours to 7 days). Foraminifera biovolume was calculated on the basis of test morphology using equations from de Freitas *et al.* (*92*). The rate of consumption (U) is defined here as bulk respiration rate, namely the moles of ^{13}C remineralized as $^{13}CO_2$. The average volume of the prey cells was estimated using the average cell size and carbon content of *C. socialis* (*93*).

The total amount of remineralized ^{13}C-APM is the sum of all respiration in our APM treatments and most likely includes not only foraminifera but also bacteria, archaea, fungi, and other heterotrophic protists that used the ^{13}C-APM during the incubations. Therefore, we constrained U using three different sets of assumptions (going from least to most likely): (i) 100% of the measured $^{13}CO_2$ was produced by foraminifera; (ii) 1% of the measured $^{13}CO_2$ was produced by foraminifera; and (iii) the amount $^{13}CO_2$ produced by ^{13}C-APM–remineralizing foraminifera in our treatments was proportional to the relative abundance of foraminifera 18*S* rRNA (of the total 18*S* and 16*S* rRNA) in metatranscriptomes from the same time points.

Last, our NGE calculations were grouped into oxic and anoxic categories, based on the presence (during the first 18 hours) or absence (at the 7- and 10-day time points) of O_2 in the water fraction during the APM incubations. We then compared our estimated NGEs from both categories to the predicted NGEs for aerobic and anaerobic (fermentative) protists (Fig. 3C).

Supplementary Materials

This PDF file includes:

Figs. S1 to S8

REFERENCES AND NOTES

1. H. Agić, "Origin and early evolution of the eukaryotes: Perspectives from the fossil record" in *Prebiotic Chemistry and the Origin of Life*, A. Neubeck, S. McMahon, Eds. (Springer International Publishing, 2021), pp. 255–289.
2. J. J. Brocks, B. J. Nettersheim, P. Adam, P. Schaeffer, A. J. M. Jarrett, N. Güneli, T. Liyanage, L. M. van Maldegem, C. Hallmann, J. M. Hope, Lost world of complex life and the late rise of the eukaryotic crown. *Nature* **618**, 767–773 (2023).
3. R. G. Stockey, D. B. Cole, U. C. Farrell, H. Agić, T. H. Boag, J. J. Brocks, D. E. Canfield, M. Cheng, P. W. Crockford, H. Cui, T. W. Dahl, L. Del Mouro, K. Dewing, S. Q. Dornbos, J. F. Emmings, R. R. Gaines, T. M. Gibson, B. C. Gill, G. J. Gilleaudeau, K. Goldberg, R. Guilbaud, G. Halverson, E. U. Hammarlund, K. Hantsoo, M. A. Henderson, C. M. Henderson, M. S. W. Hodgskiss, A. J. M. Jarrett, D. T. Johnston, P. Kabanov, J. Kimmig, A. H. Knoll, M. Kunzmann, M. A. LeRoy, C. Li, D. K. Loydell, F. A. Macdonald, J. M. Magnall, N. T. Mills, L. M. Och, B. O'Connell, A. Pagès, S. E. Peters, S. M. Porter, S. W. Poulton, S. R. Ritzer, A. D. Rooney, S. Schoepfer, E. F. Smith, J. V. Strauss, G. J. Uhlein, T. White, R. A. Wood, C. R. Woltz, I. Yurchenko, N. J. Planavsky, E. A. Sperling, Sustained increases in atmospheric oxygen and marine productivity in the Neoproterozoic and Palaeozoic eras. *Nat. Geosci.* **17**, 667–674 (2024).
4. T. M. Gibson, P. M. Shih, V. M. Cumming, W. W. Fischer, P. W. Crockford, M. S. W. Hodgskiss, S. Wörndle, R. A. Creaser, R. H. Rainbird, T. M. Skulski, G. P. Halverson, Precise age of Bangiomorpha pubescens dates the origin of eukaryotic photosynthesis. *Geology* **46**, 135–138 (2018).
5. J. J. Brocks, A. J. M. Jarrett, E. Sirantoine, C. Hallmann, Y. Hoshino, T. Liyanage, The rise of algae in Cryogenian oceans and the emergence of animals. *Nature* **548**, 578–581 (2017).
6. G. D. Love, J. Alex Zumberge, "Emerging patterns in proterozoic lipid biomarker records" in *Elements in Geochemical Tracers in Earth System Science* (Cambridge Univ. Press, 2021).
7. D. B. Mills, The origin of phagocytosis in Earth history. *Interface Focus* **10**, 20200019 (2020).
8. S. M. Porter, A. H. Knoll, Testate amoebae in the Neoproterozoic Era: Evidence from vase-shaped microfossils in the Chuar Group, Grand Canyon. *Paleobiology* **26**, 360–385 (2000).
9. D. J. G. Lahr, A. Kosakyan, E. Lara, E. A. D. Mitchell, L. Morais, A. L. Porfirio-Sousa, G. M. Ribeiro, A. K. Tice, T. Pánek, S. Kang, M. W. Brown, Phylogenomics and morphological reconstruction of Arcellinida testate amoebae highlight diversity of microbial eukaryotes in the neoproterozoic. *Curr. Biol.* **29**, 991–1001.e3 (2019).
10. T. Bosak, D. J. G. Lahr, S. B. Pruss, F. A. Macdonald, A. J. Gooday, L. Dalton, E. D. Matys, Possible early foraminiferans in post-Sturtian (716–635 Ma) cap carbonates. *Geology* **40**, 67–70 (2012).
11. B. J. Nettersheim, J. J. Brocks, A. Schwelm, J. M. Hope, F. Not, M. Lomas, C. Schmidt, R. Schiebel, E. C. M. Nowack, P. De Deckker, J. Pawlowski, S. S. Bowser, I. Bobrovskiy, K. Zonneveld, M. Kucera, M. Stuhr, C. Hallmann, Putative sponge biomarkers in unicellular Rhizaria question an early rise of animals. *Nat. Ecol. Evol.* **3**, 577–581 (2019).
12. G. D. Love, E. Grosjean, C. Stalvies, D. A. Fike, J. P. Grotzinger, A. S. Bradley, A. E. Kelly, M. Bhatia, W. Meredith, C. E. Snape, S. A. Bowring, D. J. Condon, R. E. Summons, Fossil steroids record the appearance of Demospongiae during the Cryogenian period. *Nature* **457**, 718–721 (2009).
13. I. Bobrovskiy, J. M. Hope, B. J. Nettersheim, J. K. Volkman, C. Hallmann, J. J. Brocks, Algal origin of sponge sterane biomarkers negates the oldest evidence for animals in the rock record. *Nat. Ecol. Evol.* **5**, 165–168 (2021).

14. M. O. Brown, B. O. Olagunju, J.-L. Giner, P. V. Welander, Sterol methyltransferases in uncultured bacteria complicate eukaryotic biomarker interpretations. *Nat. Commun.* **14**, 1859 (2023).
15. J. J. Brocks, The transition from a cyanobacterial to algal world and the emergence of animals. *Emerg. Top. Life Sci.* **2**, 181–190 (2018).
16. F. S. Dunn, A. G. Liu, D. V. Grazhdankin, P. Vixseboxse, J. Flannery-Sutherland, E. Green, S. Harris, P. R. Wilby, P. C. J. Donoghue, The developmental biology of *Charnia* and the eumetazoan affinity of the Ediacaran rangeomorphs. *Sci. Adv.* **7**, eabe0291 (2021).
17. A. H. Knoll, D. J. G. Lahr, "Fossils, feeding, and the evolution of complex multicellularity" in *Multicellularity, Origins and Evolution, The Vienna Series in Theoretical Biology: Boston, Massachusetts Institute of Technology,* The MIT Press, (2016), pp. 1–16.
18. C. Wang, M. A. Lechte, C. T. Reinhard, D. Asael, D. B. Cole, G. P. Halverson, S. M. Porter, N. Galili, I. Halevy, R. H. Rainbird, T. W. Lyons, N. J. Planavsky, Strong evidence for a weakly oxygenated ocean–atmosphere system during the Proterozoic. *Proc. Natl. Acad. Sci. U.S.A.* **119**, e2116101119 (2022).
19. T. Fenchel, B. J. Finlay, *Ecology and Evolution in Anoxic Worlds*, Oxford Series in Ecology and Evolution (Oxford Univ. Press, 1995).
20. A. V. Altenbach, J. M. Bernhard, J. Seckbach, *Anoxia: Evidence for Eukaryote Survival and Paleontological Strategies* (Springer, 2011).
21. N. Glock, A.-S. Roy, D. Romero, T. Wein, J. Weissenbach, N. P. Revsbech, S. Høgslund, D. Clemens, S. Sommer, T. Dagan, Metabolic preference of nitrate over oxygen as an electron acceptor in foraminifera from the Peruvian oxygen minimum zone. *Proc. Natl. Acad. Sci. U.S.A.* **116**, 2860–2865 (2019).
22. W. D. Orsi, R. Morard, A. Vuillemin, M. Eitel, G. Wörheide, J. Milucka, M. Kucera, Anaerobic metabolism of Foraminifera thriving below the seafloor. *ISME J.* **14**, 2580–2594 (2020).
23. J. S. Graf, S. Schorn, K. Kitzinger, S. Ahmerkamp, C. Woehle, B. Huettel, C. J. Schubert, M. M. M. Kuypers, J. Milucka, Anaerobic endosymbiont generates energy for ciliate host by denitrification. *Nature* **591**, 445–450 (2021).
24. C. Woehle, A.-S. Roy, N. Glock, J. Michels, T. Wein, J. Weissenbach, D. Romero, C. Hiebenthal, S. N. Gorb, J. Schönfeld, T. Dagan, Denitrification in foraminifera has an ancient origin and is complemented by associated bacteria. *Proc. Natl. Acad. Sci. U.S.A.* **119**, e2200198119 (2022).
25. T. Fenchel, The microbial loop – 25 years later. *J. Exp. Mar. Bio. Ecol.* **366**, 99–103 (2008).
26. C. Schmoker, S. Hernández-León, A. Calbet, Microzooplankton grazing in the oceans: Impacts, data variability, knowledge gaps and future directions. *J. Plankton Res.* **35**, 691–706 (2013).
27. D. K. Stoecker, M. D. Johnson, C. de Vargas, Acquired phototrophy in aquatic protists. *Aquat. Microb. Ecol.* **57**, 279–310 (2009).
28. T. Fenchel, B. J. Finlay, Anaerobic free-living protozoa: Growth efficiencies and the structure of anaerobic communities. *FEMS Microbiol. Lett.* **74**, 269–275 (1990).
29. A. Saccà, "The role of eukaryotes in the anaerobic food web of stratified lakes" in *Anoxia: Evidence for Eukaryote Survival and Paleontological Strategies*, A. V. Altenbach, J. M. Bernhard, J. Seckbach, Eds. (Springer, 2011), pp. 403–419.
30. M.-E. Carr, Estimation of potential productivity in Eastern Boundary Currents using remote sensing. *Deep Sea Res. II Top. Stud. Oceanogr.* **49**, 59–80 (2001).
31. G. C. Pitcher, Sedimentary flux and the formation of resting spores of selected *Chaetoceros* species at two sites in the southern Benguela System. *S. Afr. J. Mar. Sci.* **4**, 231–244 (1986).
32. G. C. Pitcher, S. J. Weeks, "7 The variability and potential for prediction of harmful algal blooms in the southern Benguela ecosystem" in *Large Marine Ecosystems*, V. Shannon, G. Hempel, P. Malanotte-Rizzoli, C. Moloney, J. Woods, Eds. (Elsevier, 2006), pp. 125–146, vol. 14.
33. J. Kämpf, P. Chapman, *Upwelling Systems of the World* (Springer International Publishing, 2016).
34. R. Barlow, T. Lamont, D. Louw, M.-J. Gibberd, R. Airs, A. van der Plas, Environmental influence on phytoplankton communities in the northern Benguela ecosystem. *Afr. J. Mar. Sci.* **40**, 355–370 (2018).
35. P. Pufahl, M. Maslin, L. Anderson, V. Brüchert, F. Jansen, H. Lin, M. Perez, L. Vidal, Lithostratigraphic summary for leg 175: Angola-Benguela upwelling system. *Proc. ODP. Init. Repts* **175**, 533–542 (1998).
36. W. D. Orsi, A rapid method for measuring ATP + ADP + AMP in marine sediment. *Environ. Microbiol.* **25**, 1549–1558 (2023).
37. W. S. Trimble, M. G. Coppolino, "Phagosome Maturation" in *Molecular Mechanisms of Phagocytosis*, C. Rosales, Ed. (Springer US, 2005), pp. 133–150.
38. A. Labarre, A. Obiol, S. Wilken, I. Forn, R. Massana, Expression of genes involved in phagocytosis in uncultured heterotrophic flagellates. *Limnol. Oceanogr.* **65**, S149–S160 (2020).
39. N. Yutin, M. Y. Wolf, Y. I. Wolf, E. V. Koonin, The origins of phagocytosis and eukaryogenesis. *Biol. Direct* **4**, 9 (2009).
40. D. A. Caron, P. D. Countway, P. Savai, R. J. Gast, A. Schnetzer, S. D. Moorthi, M. R. Dennett, D. M. Moran, A. C. Jones, Defining DNA-based operational taxonomic units for microbial-eukaryote ecology. *Appl. Environ. Microbiol.* **75**, 5797–5808 (2009).
41. M. Müller, M. Mentel, J. J. van Hellemond, K. Henze, C. Woehle, S. B. Gould, R.-Y. Yu, M. van der Giezen, A. G. M. Tielens, W. F. Martin, Biochemistry and evolution of anaerobic energy metabolism in eukaryotes. *Microbiol. Mol. Biol. Rev.* **76**, 444–495 (2012).
42. B. J. Finlay, A. S. W. Span, J. M. P. Harman, Nitrate respiration in primitive eukaryotes. *Nature* **303**, 333–336 (1983).
43. H. Shoun, D. H. Kim, H. Uchiyama, J. Sugiyama, Denitrification by fungi. *FEMS Microbiol. Lett.* **73**, 277–281 (1992).
44. W. D. Orsi, A. Vuillemin, Ö. K. Coskun, P. Rodriguez, Y. Oertel, J. Niggemann, V. Mohrholz, G. V. Gomez-Saez, Carbon assimilating fungi from surface ocean to subseafloor revealed by coupled phylogenetic and stable isotope analysis. *ISME J.* **16**, 1245–1261 (2022).
45. T. Fenchel, B. J. Finlay, A. Giannì, Microaerophily in ciliates: Responses of an *Euplotes* species (hypotrichida) to oxygen tension. *Archiv für Protistenkunde* **137**, 317–330 (1989).
46. C. Woehle, A.-S. Roy, N. Glock, T. Wein, J. Weissenbach, P. Rosenstiel, C. Hiebenthal, J. Michels, J. Schönfeld, T. Dagan, A novel eukaryotic denitrification pathway in Foraminifera. *Curr. Biol.* **28**, 2536–2543.e5 (2018).
47. T. Cavalier-Smith, E. E. Chao, R. Lewis, Multigene phylogeny and cell evolution of chromist infrakingdom Rhizaria: Contrasting cell organisation of sister phyla Cercozoa and Retaria. *Protoplasma* **255**, 1517–1574 (2018).
48. S. M. Porter, "The proterozoic fossil record of heterotrophic eukaryotes" in *Neoproterozoic Geobiology* and *Paleobiology*, S. Xiao, A. J. Kaufman, Eds. (Springer, 2006), pp. 1–21.
49. L. W. Parfrey, D. J. G. Lahr, A. H. Knoll, L. A. Katz, Estimating the timing of early eukaryotic diversification with multigene molecular clocks. *Proc. Natl. Acad. Sci. U.S.A.* **108**, 13624–13629 (2011).
50. H. C. Betts, M. N. Puttick, J. W. Clark, T. A. Williams, P. C. J. Donoghue, D. Pisani, Integrated genomic and fossil evidence illuminates life's early evolution and eukaryote origin. *Nat. Ecol. Evol.* **2**, 1556–1562 (2018).
51. J. F. H. Strassert, I. Irisarri, T. A. Williams, F. Burki, A molecular timescale for eukaryote evolution with implications for the origin of red algal-derived plastids. *Nat. Commun.* **12**, 3574 (2021).
52. A. L. Porfirio-Sousa, A. K. Tice, L. Morais, G. M. Ribeiro, Q. Blandenier, K. Dumack, Y. Eglit, N. W. Fry, M. B. G. E. Souza, T. C. Henderson, F. Kleitz-Singleton, D. Singer, M. W. Brown, D. J. G. Lahr, Amoebozoan testate amoebae illuminate the diversity of heterotrophs and the complexity of ecosystems throughout geological time. *Proc. Natl. Acad. Sci. U.S.A.* **121**, e2319628121 (2024).
53. N. Bremer, F. D. K. Tria, J. Skejo, S. G. Garg, W. F. Martin, Ancestral state reconstructions trace mitochondria but not phagocytosis to the last eukaryotic common ancestor. *Genome Biol. Evol.* **14**, evac079 (2022).
54. W. F. Martin, Too much eukaryote LGT. *Bioessays* **39**, 1700115 (2017).
55. M. M. Leger, L. Eme, C. W. Stairs, A. J. Roger, Demystifying eukaryote lateral gene transfer (response to Martin 2017 DOI: 10.1002/bies.201700115). *Bioessays* **40**, e1700242 (2018).
56. D. B. Mills, R. A. Boyle, S. J. Daines, E. A. Sperling, D. Pisani, P. C. J. Donoghue, T. M. Lenton, Eukaryogenesis and oxygen in Earth history. *Nat. Ecol. Evol.* **6**, 520–532 (2022).
57. C. W. Stairs, M. M. Leger, A. J. Roger, Diversity and origins of anaerobic metabolism in mitochondria and related organelles. *Philos. Trans. R. Soc. Lond. B Biol. Sci.* **370**, 20140326 (2015).
58. V. Hampl, A. J. Roger, "The evolutionary origin of mitochondria and mitochondrion-related organelles" in *Endosymbiotic Organelle Acquisition* (Springer International Publishing, 2024), pp. 89–121.
59. D. E. Canfield, E. Kristensen, B. Thamdrup, Microbial ecosystems. *Adv. Mar. Biol.* , (2005).
60. G. J. Dick, S. L. Grim, J. M. Klatt, Controls on O_2 production in cyanobacterial mats and implications for Earth's oxygenation. *Annu. Rev. Earth Planet. Sci.* **46**, 123–147 (2018).
61. E. A. Sperling, A. H. Knoll, P. R. Girguis, The ecological physiology of Earth's second oxygen revolution. *Annu. Rev. Ecol. Evol. Syst.* **46**, 215–235 (2015).
62. C. T. Reinhard, N. J. Planavsky, B. C. Gill, K. Ozaki, L. J. Robbins, T. W. Lyons, W. W. Fischer, C. Wang, D. B. Cole, K. O. Konhauser, Evolution of the global phosphorus cycle. *Nature* **541**, 386–389 (2017).
63. K. Bergmann, N. Boekelheide, J. W. Clarke, M. D. Cantine, J. Wilcots, N. T. Anderson, A. B. Jost, O. Laub, J. Drozd, S. L. Goldberg, T. Mackey, F. Meyer, A. Eyster, A billion years of temperature variability: A key driver of Earth's long-term habitability. *ESS Open Archive*, 10.1002/essoar.10511918.1 (2022).
64. P. W. Crockford, Y. M. Bar On, L. M. Ward, R. Milo, I. Halevy, The geologic history of primary productivity. *Curr. Biol.* **33**, 4741–4750.e5 (2023).
65. A. H. Knoll, R. E. Summons, J. R. Waldbauer, J. E. Zumberge, "The geological succession of primary producers in the oceans" in *Evolution of Primary Producers in the Sea*, P. G. Falkowski, A. H. Knoll, Eds. (Elsevier, 2007), pp. 133–163.
66. O. Romero, B. Boeckel, B. Donner, G. Lavik, G. Fischer, G. Wefer, Seasonal productivity dynamics in the pelagic central Benguela System inferred from the flux of carbonate and silicate organisms. *J. Mar. Syst.* **37**, 259–278 (2002).
67. S. Zhang, J. Su, S. Ma, H. Wang, X. Wang, K. He, H. Wang, D. E. Canfield, Eukaryotic red and green algae populated the tropical ocean 1400 million years ago. *Precambrian Res.* **357**, 106166 (2021).

68. A. M. C. Bowles, C. J. Williamson, T. A. Williams, T. M. Lenton, P. C. J. Donoghue, The origin and early evolution of plants. *Trends Plant Sci.* **28**, 312–329 (2023).
69. C. T. Reinhard, N. J. Planavsky, B. A. Ward, G. D. Love, G. Le Hir, A. Ridgwell, The impact of marine nutrient abundance on early eukaryotic ecosystems. *Geobiology* **18**, 139–151 (2020).
70. L. K. Eckford-Soper, D. E. Canfield, The global explosion of eukaryotic algae: The potential role of phosphorus? *PLOS ONE* **15**, e0234372 (2020).
71. D. B. Mills, R. L. Simister, T. R. Sehein, S. J. Hallam, E. A. Sperling, S. A. Crowe, Constraining the oxygen requirements for modern microbial eukaryote diversity. *Proc. Natl. Acad. Sci. U.S.A.* **121**, e2303754120 (2024).
72. J. Kang, B. Gill, R. Reid, F. Zhang, S. Xiao, Nitrate limitation in early Neoproterozoic oceans delayed the ecological rise of eukaryotes. *Sci. Adv.* **9**, eade9647 (2023).
73. T. M. Lenton, S. J. Daines, The effects of marine eukaryote evolution on phosphorus, carbon and oxygen cycling across the Proterozoic-Phanerozoic transition. *Emerg. Top. Life Sci.* **2**, 267–278 (2018).
74. P. A. Cohen, R. B. Kodner, The earliest history of eukaryotic life: Uncovering an evolutionary story through the integration of biological and geological data. *Trends Ecol. Evol.* **37**, 246–256 (2022).
75. E. A. Sperling, K. J. Peterson, M. Laflamme, Rangeomorphs, Thectardis (Porifera?) and dissolved organic carbon in the Ediacaran oceans. *Geobiology* **9**, 24–33 (2011).
76. K. Cracknell, D. C. García-Bellido, J. G. Gehling, M. J. Ankor, S. A. F. Darroch, I. A. Rahman, Pentaradial eukaryote suggests expansion of suspension feeding in White Sea-aged Ediacaran communities. *Sci. Rep.* **11**, 4121 (2021).
77. J. G. Gehling, B. N. Runnegar, M. L. Droser, Scratch traces of large Ediacara bilaterian animals. *J. Paleo.* **88**, 284–298 (2014).
78. E. A. Sperling, J. Vinther, A placozoan affinity for Dickinsonia and the evolution of late Proterozoic metazoan feeding modes. *Evol. Dev.* **12**, 201–209 (2010).
79. L. Parry, P. Boggiani, D. Condon, R. Garwood, J. Leme, D. McIlroy, M. Brasier, R. Trindade, G. Campanha, M. L. Pacheco, C. Diniz, A. Liu, Ichnological evidence for meiofaunal bilaterians from the terminal Ediacaran and earliest Cambrian of Brazil. *Nat. Ecol. Evol.* **1**, 1455–1464 (2017).
80. R. R. L. Guillard, P. E. Hargraves, Stichochrysis immobilis is a diatom, not a chrysophyte. *Phycologia* **32**, 234–236 (1993).
81. B. Buchfink, C. Xie, D. H. Huson, Fast and sensitive protein alignment using DIAMOND. *Nat. Methods* **12**, 59–60 (2015).
82. P. J. Keeling, F. Burki, H. M. Wilcox, B. Allam, E. E. Allen, L. A. Amaral-Zettler, E. Virginia Armbrust, J. M. Archibald, A. K. Bharti, C. J. Bell, B. Beszteri, K. D. Bidle, C. T. Cameron, L. Campbell, D. A. Caron, R. A. Cattolico, J. L. Collier, K. Coyne, S. K. Davy, P. Deschamps, S. T. Dyhrman, B. Edvardsen, R. D. Gates, C. J. Gobler, S. J. Greenwood, S. M. Guida, J. L. Jacobi, K. S. Jakobsen, E. R. James, B. Jenkins, U. John, M. D. Johnson, A. R. Juhl, A. Kamp, L. A. Katz, R. Kiene, A. Kudryavtsev, B. S. Leander, S. Lin, C. Lovejoy, D. Lynn, A. Marchetti, G. McManus, A. M. Nedelcu, S. Menden-Deuer, C. Miceli, T. Mock, M. Montresor, M. A. Moran, S. Murray, G. Nadathur, S. Nagai, P. B. Ngam, B. Palenik, J. Pawlowski, G. Petroni, G. Piganeau, M. C. Posewitz, K. Rengefors, G. Romano, M. E. Rumpho, T. Rynearson, K. B. Schilling, D. C. Schroeder, A. G. B. Simpson, C. H. Slamovits, D. R. Smith, G. Jason Smith, S. R. Smith, H. M. Sosik, P. Stief, E. Theriot, S. N. Twary, P. E. Umale, D. Vaulot, B. Wawrik, G. L. Wheeler, W. H. Wilson, Y. Xu, A. Zingone, A. Z. Worden, The Marine Microbial Eukaryote Transcriptome Sequencing Project (MMETSP): Illuminating the functional diversity of eukaryotic life in the oceans through transcriptome sequencing. *PLOS Biol.* **12**, e1001889 (2014).
83. E. V. Koonin, N. D. Fedorova, J. D. Jackson, A. R. Jacobs, D. M. Krylov, K. S. Makarova, R. Mazumder, S. L. Mekhedov, A. N. Nikolskaya, B. S. Rao, I. B. Rogozin, S. Smirnov, A. V. Sorokin, A. V. Sverdlov, S. Vasudevan, Y. I. Wolf, J. J. Yin, D. A. Natale, A comprehensive evolutionary classification of proteins encoded in complete eukaryotic genomes. *Genome Biol.* **5**, R7 (2004).
84. S. J. Salter, M. J. Cox, E. M. Turek, S. T. Calus, W. O. Cookson, M. F. Moffatt, P. Turner, J. Parkhill, N. J. Loman, A. W. Walker, Reagent and laboratory contamination can critically impact sequence-based microbiome analyses. *BMC Biol.* **12**, 87 (2014).
85. J. Tamames, F. Puente-Sánchez, SqueezeMeta, A highly portable, fully automatic metagenomic analysis pipeline. *Front. Microbiol.* **9**, 3349 (2018).
86. C. Quast, E. Pruesse, P. Yilmaz, J. Gerken, T. Schweer, P. Yarza, J. Peplies, F. O. Glöckner, The SILVA ribosomal RNA gene database project: Improved data processing and web-based tools. *Nucleic Acids Res.* **41**, D590–D596 (2013).
87. L. Guillou, D. Bachar, S. Audic, D. Bass, C. Berney, L. Bittner, C. Boutte, G. Burgaud, C. de Vargas, J. Decelle, J. Del Campo, J. R. Dolan, M. Dunthorn, B. Edvardsen, M. Holzmann, W. H. C. F. Kooistra, E. Lara, N. Le Bescot, R. Logares, F. Mahé, R. Massana, M. Montresor, R. Morard, F. Not, J. Pawlowski, I. Probert, A.-L. Sauvadet, R. Siano, T. Stoeck, D. Vaulot, P. Zimmermann, R. Christen, The Protist Ribosomal Reference database (PR2): A catalog of unicellular eukaryote small sub-unit rRNA sequences with curated taxonomy. *Nucleic Acids Res.* **41**, D597–D604 (2013).
88. J. del Campo, M. Kolisko, V. Boscaro, L. F. Santoferrara, S. Nenarokov, R. Massana, L. Guillou, A. Simpson, C. Berney, C. de Vargas, M. W. Brown, P. J. Keeling, L. Wegener Parfrey, EukRef: Phylogenetic curation of ribosomal RNA to enhance understanding of eukaryotic diversity and distribution. *PLOS Biol.* **16**, e2005849 (2018).
89. R. C. Edgar, MUSCLE: A multiple sequence alignment method with reduced time and space complexity. *BMC Bioinformatics* **5**, 113 (2004).
90. M. Gouy, S. Guindon, O. Gascuel, SeaView version 4: A multiplatform graphical user interface for sequence alignment and phylogenetic tree building. *Mol. Biol. Evol.* **27**, 221–224 (2010).
91. S. Guindon, J.-F. Dufayard, V. Lefort, M. Anisimova, W. Hordijk, O. Gascuel, New algorithms and methods to estimate maximum-likelihood phylogenies: Assessing the performance of PhyML 3.0. *Syst. Biol.* **59**, 307–321 (2010).
92. T. R. de Freitas, E. T. Bacalhau, S. T. Disaró, Biovolume method for foraminiferal biomass assessment: Evaluation of geometric models and incorporation of species mean cell occupancy. *J. Foraminiferal Res.* **51**, 249–266 (2021).
93. B. C. Booth, P. Larouche, S. Bélanger, B. Klein, D. Amiel, Z.-P. Mei, Dynamics of *Chaetoceros* socialis blooms in the North Water. *Deep Sea Res. II Top. Stud. Oceanogr.* **49**, 5003–5025 (2002).
94. W. F. Martin, A. G. M. Tielens, M. Mentel, S. G. Garg, S. B. Gould, The physiology of phagocytosis in the context of mitochondrial origin. *Microbiol. Mol. Biol. Rev.* **81**, e00008-17 (2017).
95. B. S. Leander, Did trypanosomatid parasites have photosynthetic ancestors? *Trends Microbiol.* **12**, 251–258 (2004).
96. M. Laflamme, S. Xiao, M. Kowalewski, Osmotrophy in modular Ediacara organisms. *Proc. Natl. Acad. Sci. U.S.A.* **106**, 14438–14443 (2009).

Acknowledgments: We thank the captain and crew of the *F/S* Meteor (M148/2 EreBUS) for assisting this oceanographic expedition, as well as S. Littmann, T. Wilkop, G. Klockgether, and K. Imhoff for helping obtain samples. We also gratefully acknowledge the work of T. Fenchel and B. Finlay. **Funding:** We acknowledge funding from the Deutsche Forschungsgemeinschaft (DFG) through Project OR 417/7-1 (granted to W.D.O.). **Author contributions:** Conceptualization: D.B.M. and W.D.O. Data curation: D.B.M. and W.D.O. Formal analysis: D.B.M., K.M., W.D.O., and A.V. Funding acquisition: W.D.O. Investigation: K.M. and W.D.O. Methodology: D.B.M., W.D.O., and A.V. Project administration: W.D.O. Resources: D.B.M. and W.D.O. Software: D.B.M., W.D.O., and A.V. Supervision: W.D.O. Validation: D.B.M. and W.D.O. Visualization: D.B.M. and W.D.O. Writing—original draft: D.B.M. and W.D.O. Writing—review and editing: Ö.K.C., D.B.M., W.D.O., and A.V. **Competing interests:** The authors declare that they have no competing interests. **Data and materials availability:** All data needed to evaluate the conclusions in the paper are present in the paper and/or the Supplementary Materials. All metatranscriptome data are publicly accessible in NCBI through BioProject number PRJNA525353.

Submitted 17 September 2024
Accepted 16 January 2025
Published 19 February 2025
10.1126/sciadv.adt2147